

1. Introduction

HERA is ESA's first planetary defense mission, launched last 7th October 2024 as part of the joint ESA-NASA AIDA collaboration. It will reach the Didymos binary asteroid system in October 2026 [1].

In March 2025, HERA performed a Mars flyby, during which Earth-based radiometric data and optical images of the planet, Deimos and Phobos, were acquired. Providing an opportunity to test and validate optical navigation (OPNAV) image-processing pipelines and orbit determination algorithms.

This poster presents an OPNAV image-processing pipeline developed for the HERA mission. The pipeline performs a calibration of the Asteroid Framing Cameras (AFCs) using star-field images, then extracts Deimos center-of-figure from images of the Mars flyby. ARAGO software, based on Caviar [2], is used to find star centroids and then determine the moons' astrometric points. These OPNAV measurements are then incorporated into an Orbit Determination (OD) process.

2. Camera Model

The parameters of the AFCs that were used as nominal reference for the calibration analysis come from HERA calibration report [3]. The pinhole camera model is used in the Acton-Duxbury formulation [4] for the distortion representation. From gnomonic projection:

$$\begin{pmatrix} x \\ y \end{pmatrix} = f/A_3 \begin{pmatrix} A_1 \\ A_2 \end{pmatrix}$$

Converted in pixel (shortened version):

$$\begin{pmatrix} p \\ l \end{pmatrix} = \begin{pmatrix} K_x & K_{xy} \\ K_{yx} & K_y \end{pmatrix} \begin{pmatrix} x + \Delta x \\ y + \Delta y \end{pmatrix} + \begin{pmatrix} p_0 \\ l_0 \end{pmatrix}$$

Where:

$$\begin{pmatrix} \Delta x \\ \Delta y \end{pmatrix} = \begin{pmatrix} xr^2 & xy & x^2 \\ yr^2 & y^2 & xy \end{pmatrix} \begin{pmatrix} \alpha_1 \\ \alpha_4 \\ \alpha_5 \end{pmatrix}$$

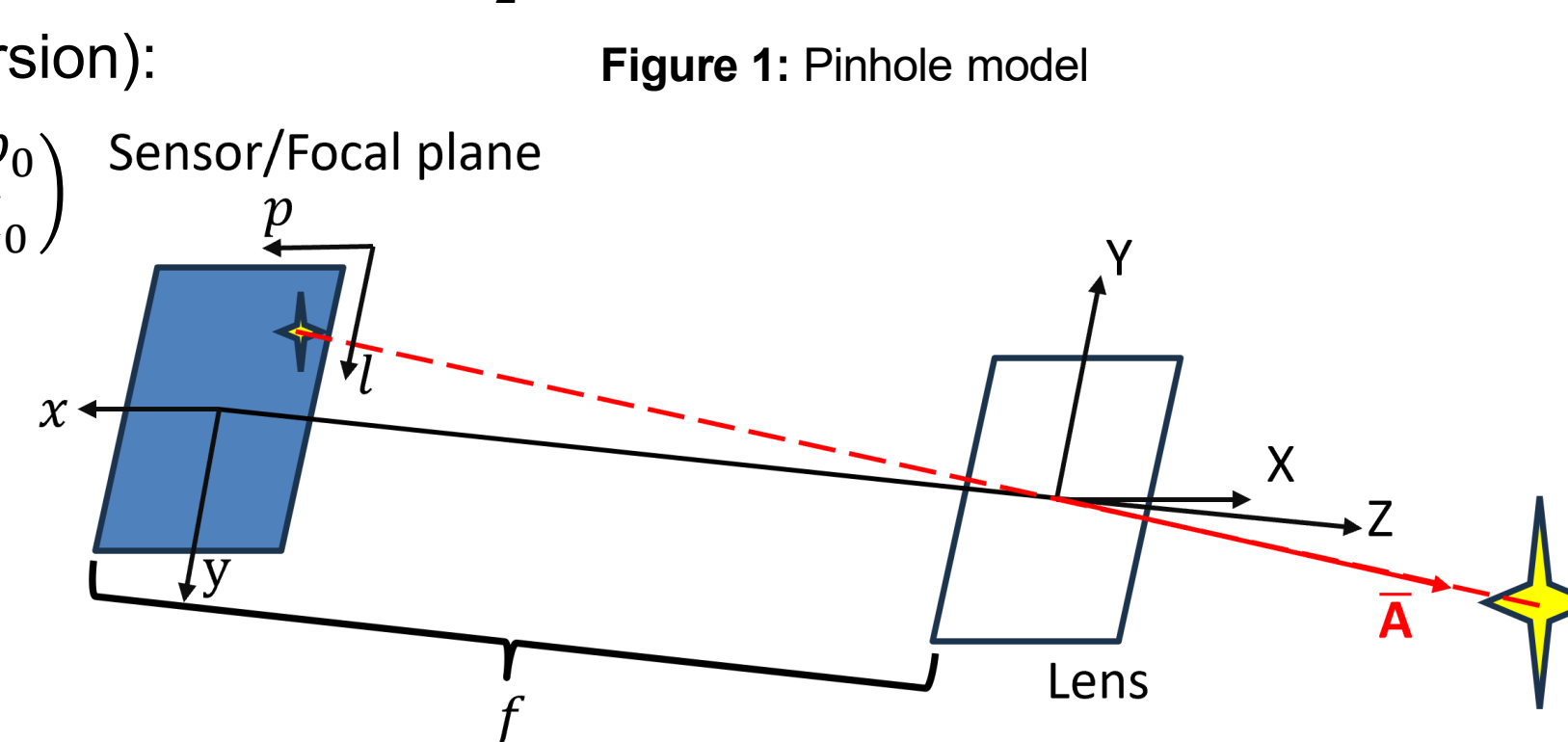


Figure 1: Pinhole model

3. AFCs Calibration Pipeline

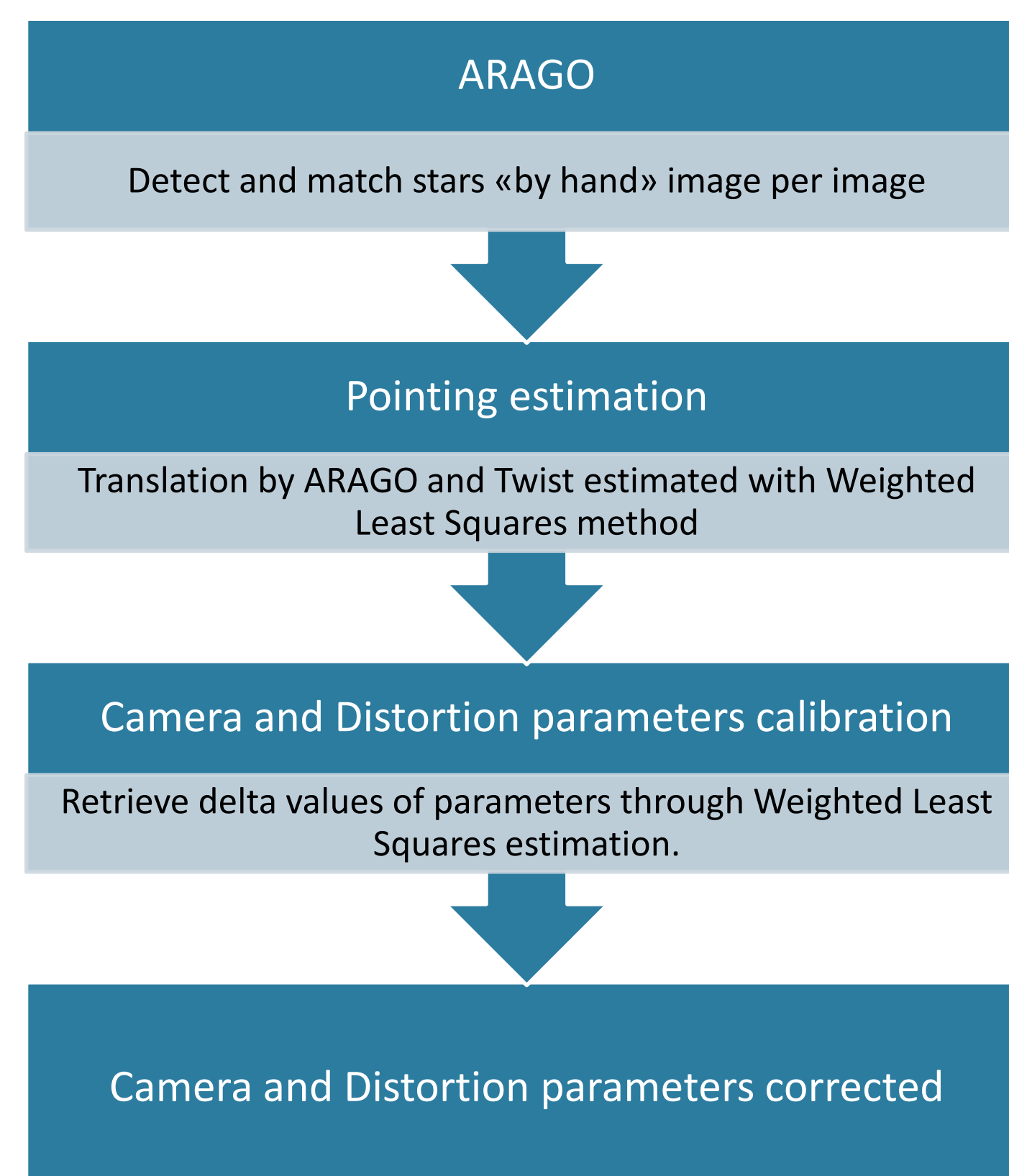


Figure 2: Scheme of the calibration pipeline.

The objective of the calibration pipeline is to estimate the precise pointing of the camera and its intrinsic parameters, by minimizing the residuals between observed and computed stars position in the images.

In this analysis only four parameters were estimated:

- f (focal length),
- α_1 (radial distortion parameter),
- α_4 and α_5 (tip and tilt).

ARAGO initializes the pipeline finding the stars in the images and determining their centroid position, among others, through the Photogravity Center Method [5,6].

4. Image-Processing Pipeline

After the calibration, the image-processing pipeline follows the following steps [7]:

1. Star detection and star matching.
2. Limb detection.
3. Projection onto the picture of the predicted body shape.
4. LSQ limb fitting between detected limb and the predicted shape.
5. Centroid estimation using the predicted shape data.

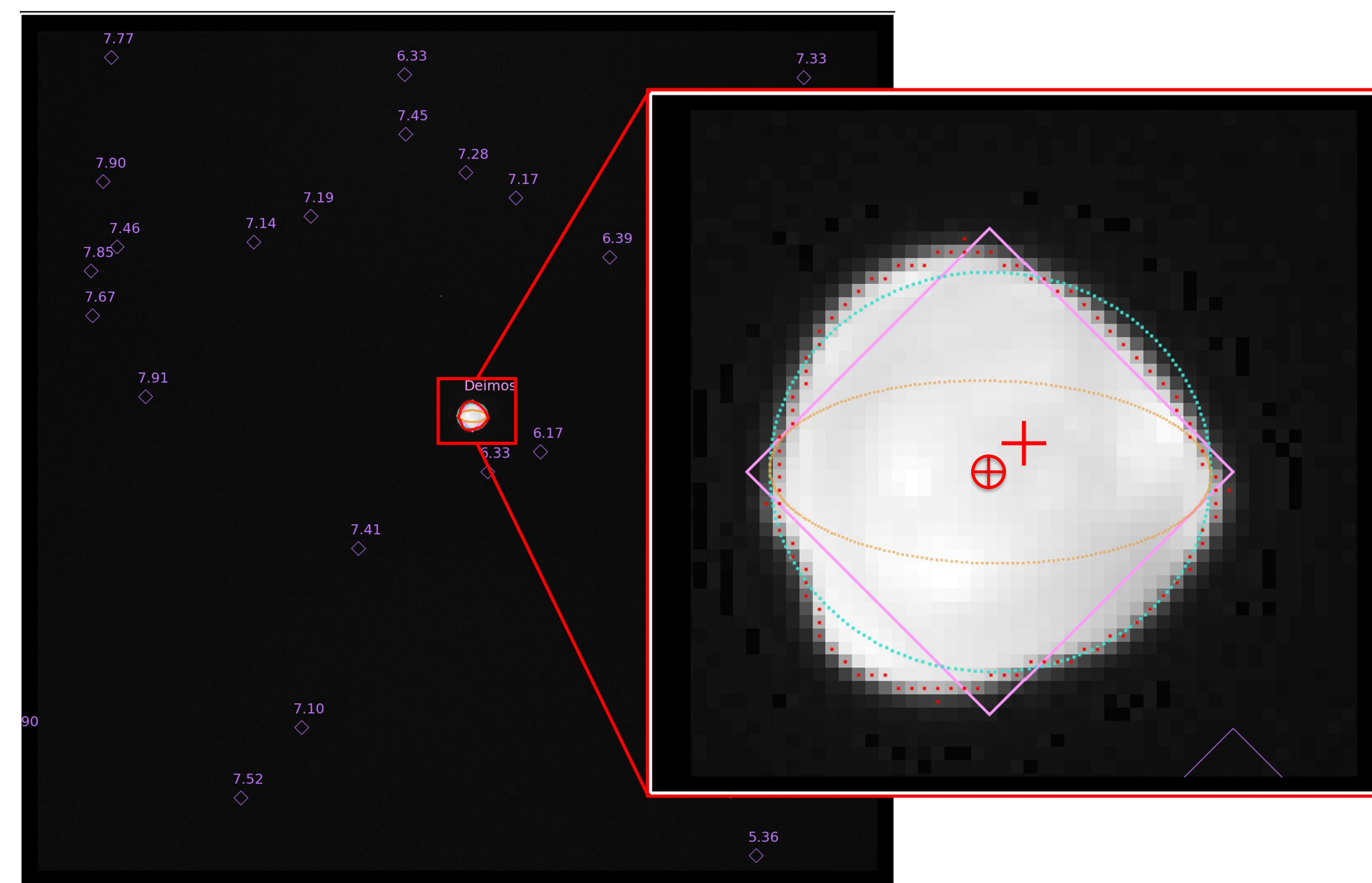


Figure 3: Image of Deimos processed with ARAGO. A limb detection algorithm finds the limb points (red) and an ellipse fitting has been performed using the Deimos ellipsoidal shape (cyan) computed from kernels, to determine its centroid (circle cross).

5. Orbit Determination Process

HERA performed the Mars Flyby last 12th March 2025. Between the 11:52:31 and 13:25:10 UTC the spacecraft took images of Deimos and Phobos, before and after the Mars Closest Approach, respectively.

The OD process aims at reconstructing the spacecraft trajectory with high accuracy by combining radiometric and optical measurements. OPNAV measurements are obtained from images of Deimos and Phobos, where the observed sample and line coordinates of the image's centroids provide line-of-sight constraints. These measurements can also contribute to refining the ephemerides of the observed bodies.

OD Setup

- Ephemeris: mar099 [8], DE440 [9], SB441 (asteroids).
- Mars Fixed Frame IAU2015.
- HERA initial state and attitude from kernels.
- Star catalog constructed merging GaiaDR3 [10] and Tycho [11] star data.

OPNAV Uncertainties

- Stars: $\sigma_p = 0.181$, $\sigma_l = 0.149$ (worst cases from calibration)
- Body centroid [12]: $\sigma^2 = \sigma_b^2 + (D_{(pixel)} \cdot C)^2$

The OD is performed using NASA-JPL's library MONTE (Mission Analysis, Operations, and Navigation Toolkit Environment) [13].

6. Calibration Results

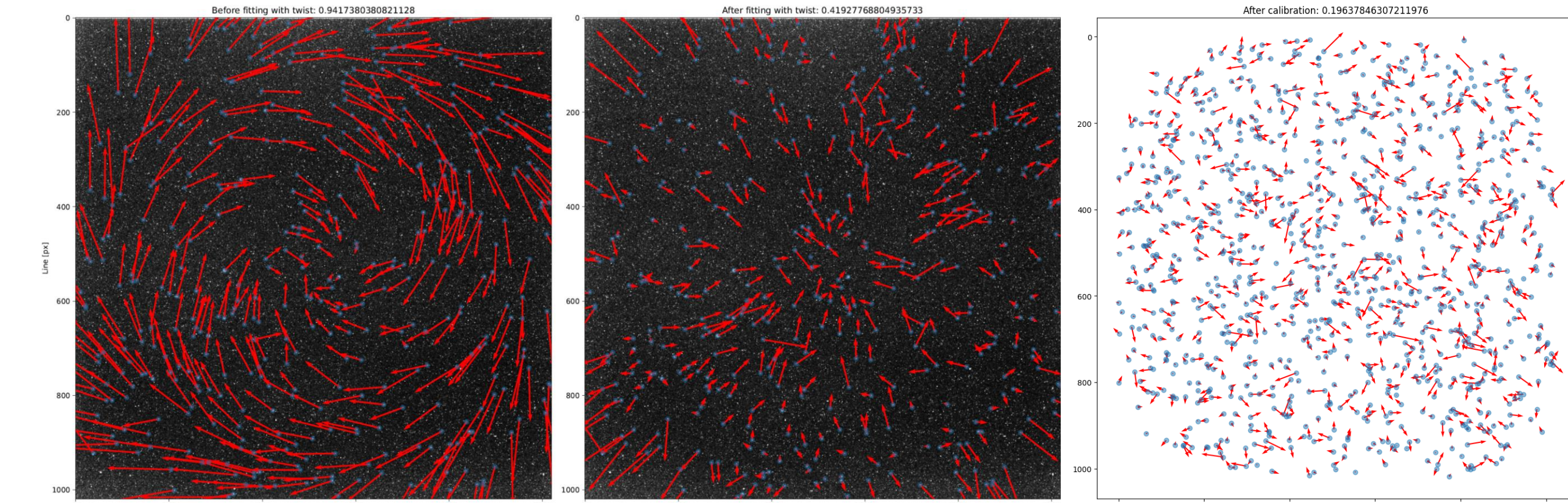


Figure 4: Examples of AFC-1 pointing correction and calibration. Arrows represent the magnitude and the direction of the residuals from computed to observed stars. First two images represent residuals before and after the pointing correction. The third image shows residuals after the estimation of the intrinsic parameters.

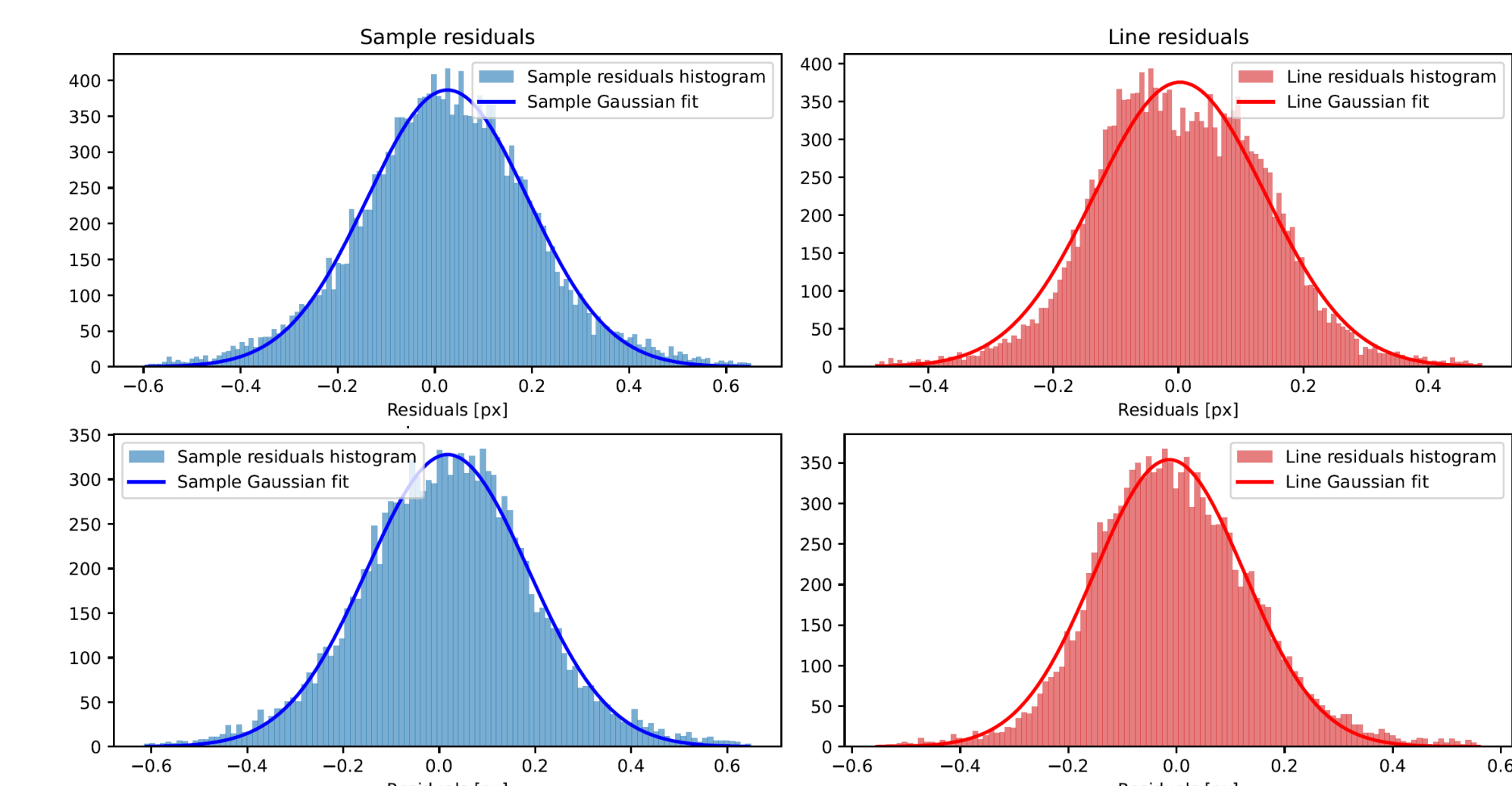


Figure 5: Final residuals distribution for AFC-1 in the first row and AFC-2 in the second row.

Tables: Left table: mean pointing correction among all images analysed. Right table: results of the calibration as difference wrt the nominal value.

	Sample [px]	Line [px]	Twist [rad]	Focal length [mm]	a1 [mm ²]	a4 [mm ⁻¹]	a5 [mm ⁻¹]
Nominal	0	0	0	105.8	0	0	0
AFC-1 (ca. 18000 points)							
Delta Value	-0.285	1.412e-04	-1.835e-05	-5.641e-05			
Sigma	1.114e-03	4.831e-07	1.211e-06	1.213e-06			
AFC-2 (ca. 12000 points)							
Delta Value	-0.164	1.340e-04	9.121e-06	-1.541e-05			
Sigma	1.361e-03	5.914e-07	1.485e-06	1.456e-06			

7. OD Preliminary Results

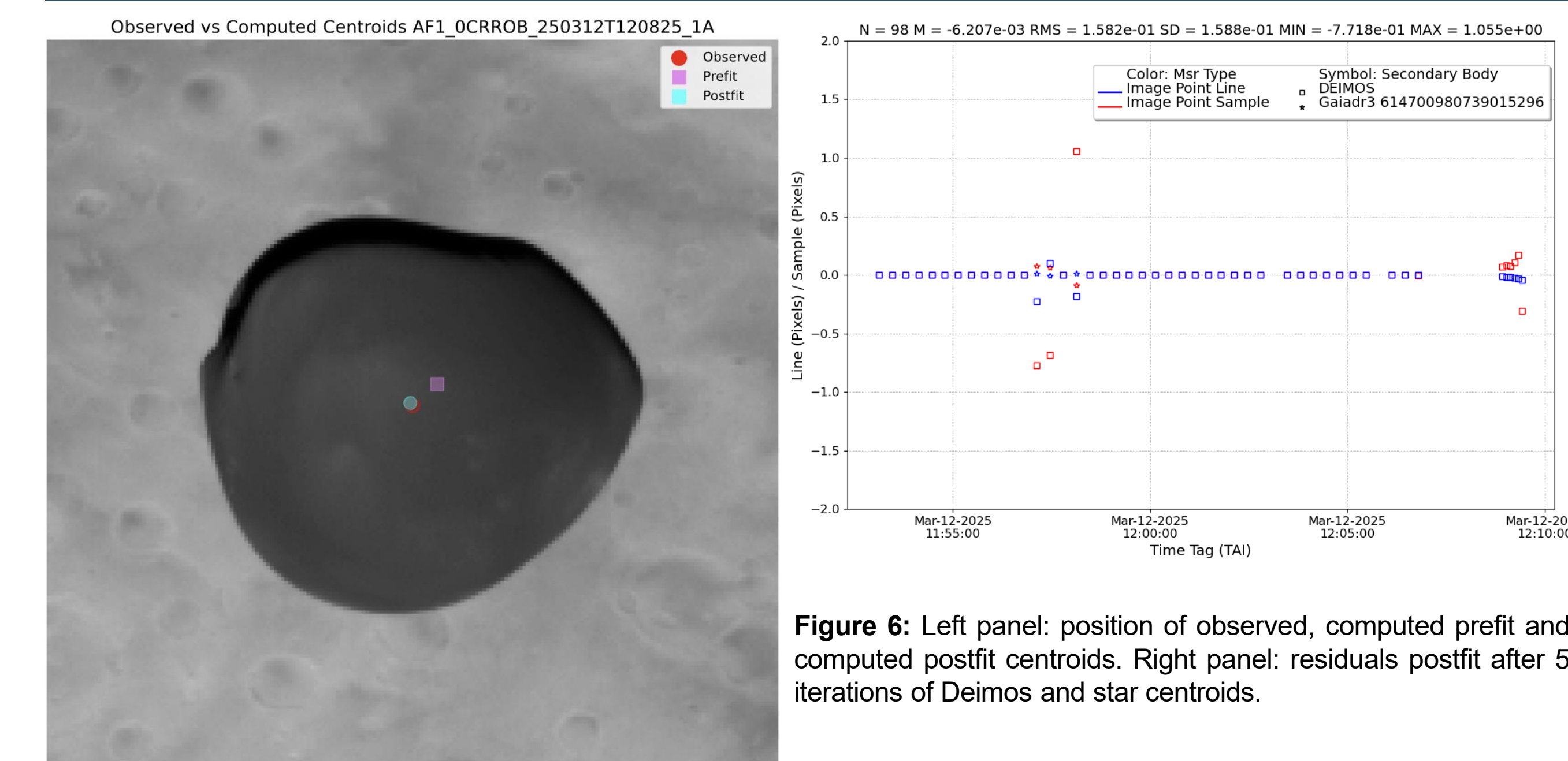


Figure 6: Left panel: position of observed, computed prefit and computed postfit centroids. Right panel: residuals postfit after 5 iterations of Deimos and star centroids.

Acknowledgements

DB, RLM, MG, EZ and PT wish to acknowledge Caltech and the NASA Jet Propulsion Laboratory for granting the University of Bologna a license to an executable version of MONTE Project Edition S/W. DB, RLM, MZ, EG and PT are grateful to the Italian Space Agency (ASI) for financial support through Agreement No. 2022-8-HH.0 in the context of ESA's Hera mission.

References

- [1] Michel, P., et al. 2022, PSJ, 3, 160.
- [2] Cooper, N. J., et al. 2018, A&A, 610, A2.
- [3] Kovács, G., & Nagy, B. V. 2024, *Hera Optical Calibration - AFC Calibration Report*, HE-BME-MOGI-DOC-011, Issue 1, Budapest University of Technology and Economics / ESA.
- [4] Owen, W. M. Jr. 2024, *Spacecraft Optical Navigation*, Wiley.
- [5] Zhang, Q. F., et al. 2021, MNRAS, 505, 5253.
- [6] Assafin, M. 2023, Planet. Space Sci., 238, 105801.

[7] Tajeddine, R., et al. 2013, A&A, 551, A129.

[8] Brozović, M., et al. 2025, AJ, 170, 42.

[9] Park, R. S., Folkner, W. M., Williams, J. G., et al. 2021, AJ, 161, 105.

[10] Gaia collaboration et al. (2023): Gaia DR3: summary of the contents and survey properties.

[11] ESA. 1997, *The Hipparcos and Tycho Catalogues*, ESA SP-1200.

[12] Jacobson, R. A., et al. 2006, AJ, 132, 2520.

[13] Evans, S., et al. 2018, CEAS Space J., 10, 79.



(*) davide.banzi4@unibo.it

- (1) Dipartimento di Ingegneria Industriale, University of Bologna, Forlì, Italy.
- (2) Centro Interdipartimentale di Ricerca Industriale Aerospaziale, University of Bologna, Forlì, Italy.
- (3) IMCCE, Observatoire de Paris, PSL Research University, Sorbonne Université, CNRS, Univ. Lille: 77 avenue Denfert Rochereau, 75014 Paris, France.

This presentation participates in OSPP



Outstanding Student & PhD candidate Presentation contest

